Computers & Fluids 86 (2013) 500–509

Contents lists available at ScienceDirect

Computers & Fluids

journal homepage: www.elsevier.com/locate/compfluid

Effect of side confining walls on the growth rate of compressible mixing layers

Afroz Javed [a], N.K.S. Rajan [b], Debasis Chakraborty [a,*]

[a] Directorate of Computational Dynamics, Defence Research and Development Laboratory, Kanchanbagh P.O., Hyderabad 500058, India
[b] Dept. of Aerospace Engineering, Indian Institute of Science, Bangalore 560012, India

ARTICLE INFO

Article history:
Received 25 April 2013
Accepted 29 July 2013
Available online 11 August 2013

Keywords:
Compressible mixing layer
Model free simulation
Side wall confinement

ABSTRACT

Model free simulations are performed to study the effect of the presence of side wall in compressible mixing of two parallel dissimilar gaseous streams with significant temperature difference. The turbulence statistics shows the three dimensional nature of the flow with and without the presence of side walls. The presence of side wall neither makes the flow field two dimensional, nor suppresses three dimensional disturbances. However, the comparison of shear layer growth rate and wall pressures reveal a better match with the two dimensional simulation results. This better match is explained on the basis of formation of oblique structures due to the presence of side walls which also suppress the distribution of momentum in third direction making the pressures to be higher as compared with the case without side walls.

1. Introduction

In a hypersonic air breathing vehicle, scramjet engine remains only option for propulsion system. The better understanding of mixing and combustion process in the scramjet combustor is one of the critical areas for its development. One of the main technological challenges in the development of scramjet engines is the effective mixing of air and fuel in the combustor at compressible (supersonic) conditions. The combination of very short residence times and poor mixing caused due to compressibility makes the problem difficult to solve. 'Planar confined compressible shear layer' is considered as a canonical problem to study the parallel injection in the scramjet combustor.

Most of the studies related to mixing layers have been carried out on free mixing layers which do not have any wall interaction. In practical scramjet combustors with rectangular cross sections, the fuel and oxidiser (air) mixing streams are confined in the top and bottom direction as well as in the sides. The effects of these walls have been studied using stability analysis and numerical simulations. For a shear layer inside a rectangular channel, Tam and Hu [1] showed that the coupling between the motion of the shear layer and the acoustic modes of the channel produces new instability mechanism called as 'supersonic instability' different form Kelvin–Helmholtz instability for the spatially growing mixing layers. Greenough et al. [2] have also shown two general types of instabilities: confined Kelvin–Helmholtz mode and supersonic wall modes, by analysing the effect of wall on a confined compressible temporal mixing layer. Zhuang et al. [3] carried out instability analysis for confined mixing layer and they argued that the increased instability of the confined mixing layer was due to the feedback mechanism between the growing supersonic shear layer and the wave system (wall reflections) that makes the shear layer more unstable, than the corresponding free supersonic shear layer, which loses energy to acoustic radiation to the far field. The amplification rates of the two-dimensional (bounded) and three-dimensional (free) supersonic instability modes were also compared with the experimental data by Zhuang et al. [3], and it was observed that the two dimensional results are in much better agreement with the experimental data. Morris et al. [4] further showed that the choice of width-to-height ratio of the confining duct may determine whether the two- or three-dimensional mode has a greater growth rate. The effect of lateral confining walls is studied by Chakraborty [5], a comparison of the mixing layer thickness for both laterally confined and free mixing layer are made. The thicknesses are found to be more for the confined case than those for free cases. The shock reflections from these top and bottom confining walls make the laterally confined shear layer more unstable and thus the growth starts earlier than the free counterpart, resulting in higher thickness at the same streamwise location with the growth rate remaining almost the same. Recently, Javed et al. [6] carried out both two and three-dimensional spatiotemporal simulations employing higher order finite difference scheme as well as finite volume scheme based on open source software (OpenFOAM) to understand the effect of three-dimensionality on the development of mixing layer. It is observed that although the instantaneous structures exhibit

* Corresponding author. Tel.: +91 40 24583310; fax: +91 40 24340037.
E-mail address: debasis_cfd@drdl.drdo.in (D. Chakraborty).

0045-7930/$ - see front matter © 2013 Elsevier Ltd. All rights reserved.
http://dx.doi.org/10.1016/j.compfluid.2013.07.025

three-dimensional features, the average pressure and velocities are predominantly two-dimensional. This study shows a higher growth rate for three-dimensional mixing layer simulations in comparison with that evaluated from two-dimensional simulation results. However, a number of two dimensional numerical studies [7–10] have shown a good match with the experimentally observed growth rate, velocity and pressure data, indicating that the flow field for the mixing layer experiments carried out in a confined environment may be two-dimensional in nature. Two dimensional simulations were carried out by Lu and Wu [7] for convective Mach numbers ranging from 1.05 to 1.77. The growth rates observed numerically was compared with experimental results and found in good match. Two dimensional simulations carried out by Liou et al. [8] for convective Mach numbers ranging from 0.14 to 1.28 show a good match for the normalised growth rate with the experimental curve. Normalised growth rate is also captured nicely in the 2D simulations for $M_c = 0.2–1.0$ by Li and Fu [10] using Bhatnagar–Gross–Krook (BGK) scheme [11,12]. They have concluded that although the mean velocity field and the thickness growth rates for 2D mixing layers agreed generally well with the experimental results even though the real flow is three-dimensional, velocity fluctuation intensities and shear stresses are over predicted compared with the experimental data. Chakraborty et al. [9] have carried out a 2D model free simulations of a supersonic confined mixing layer of dissimilar gases with significant temperature differences and showed a good match of wall surface pressures with experimental results, indicating the ability of 2D simulations to predict the wall pressure of a 3D experimental flow field. For these 2D numerical studies the good comparison of growth rate at higher convective Mach numbers ($M_c > 0.6$) with the experimental results give an indication that the experimental flow field may be 2D in nature in presence of confining side walls. According to Lu and Wu [7] the side walls act as suppressors for three-dimensionality and the flow is dominated by two-dimensional disturbances and structures. This suppression of three-dimensionality by side walls could explain the better match of experimental pressures data with two-dimensional simulations data.

The experimental results for growth rates and mean quantities, which are from actual 3-dimensional flows, could be well predicted using 2D simulations, when they are conducted in the presence of confining walls. It has been argued that these side walls make the flow field more two dimensional, and due to this two dimensionality of the flow field the 2D simulations are in better agreement with the experimental results. In most of the experimental studies there is little or no information available for the two or three dimensionality of the flow field. And thus the reason for the good match of the two dimensional numerical results for mixing layer growth rate, with that with the experimental data remains debatable. In order to resolve the issues concerned with the effect of side wall on the flow field, a simulation is carried out using actual duct geometry of the experimental case studied by Erdos et al. [13] as considered in Ref. [6]. Three dimensional model free simulations are carried out for exact Erdos experimental geometry in the presence of side wall for two dissimilar gases with significant temperature differences. The flow structure for three dimensionality is examined along with the turbulence statistics, and compared with the three dimensional case without any side walls and two-dimensional simulations. The growth rates of shear layer, and wall pressures are evaluated and analysed to explain the possible effects of the presence of side wall.

2. Geometry, grids, and boundary conditions for simulations

The mixing duct for Erdos' [13] experimental study is 50.8 mm wide with a height of 25.4 mm. The duct height to width ratio comes out to be 0.5. The length of duct is 535 mm. A sketch of the experimental geometry is shown in Fig. 1 with a side view showing the duct cross section, and relevant coordinate axis convention. For numerical simulations the middle plane in z-direction is considered as symmetry plane. This results in geometry with a width of 25.4 mm, with one side in the width direction as wall and the other side as symmetry. The position $z = 0$ mm represent symmetry plane, while $z = 25.4$ mm is the location of side wall.

For the present simulations a case with the nitrogen stream as the primary flow at the lower part of the duct and the hydrogen stream as secondary flow at the upper part of the duct separated by a splitter plate are considered. The details of the flow parameters are presented in Table 1. The convective Mach number $M_c = (U_1 - U_2)/(a_1 + a_2)$, comes out to be 0.80 for this mixing layer.

A detailed study of the grid independence is presented in Ref. [6] with a 2D domain. The grid independence of the solution is demonstrated by not only comparing the average results with different grids but also comparing the spectral content of the fluctuation with different grids. The grid is stretched exponentially in the axial and lateral directions with minimum grid spacing at the inflow boundary and at the interface of the two streams to capture the initial development of the mixing layer. The wall boundary layer is resolved by taking very fine mesh near the solid wall and the grid is again stretched exponentially in the region away from the wall. The grid structure employed in the simulations has 1000 points in the axial direction with minimum grid size of 0.3 mm near the inflow boundary plane and the maximum size of 0.8 mm near the outflow boundary. In the lateral direction, 101 grid points are used with a minimum grid spacing of 0.09 mm near the interface and wall, and the maximum grid spacing is of the order of 0.5 mm in the region away from interface and wall. The ratio of this minimum grid spacing in y-direction (0.09 mm) with mixing layer width in the upstream direction ($\approx$2.0 mm) comes out to be 0.045, which according to Oh and Loth [14] was adequate to give grid independent results even with second order spatial scheme as this ratio is less than 0.05. It is to be noted that the present simulations employ a fourth order spatially accurate scheme. For 3D calculation without considering side walls, a three-dimensional computation mesh with 41 planes is formed by spanning the two-dimensional grids with an equal distance in the z-direction. The distance between two planes is kept to be 0.3 mm. For the simulations considering side walls, the computational grid in the x and y direction is kept same as that used in 3D simulations without side wall, while in the z-direction 101 grid points are used. The minimum distance is near the side wall with a value of 0.01 mm. The grid is stretched towards the symmetry plane with a maximum width of 0.3 mm. The total grid size comes out to be around 10.2 million.

The velocities at the walls and splitter plate are kept zero, and constancy of wall temperatures are employed for heat transfer. A parabolic boundary layer profile is given near the walls and the splitter plate. The boundary conditions at the sides are set as periodic boundary condition for without side wall simulations. For the case considering effect of side wall, adiabatic wall with no slip velocity boundary condition is given for side wall while the other side is made a symmetry boundary. Both the streams are given equal pressure of 27,580 Pa. Nitrogen mass fraction is set to unity for primary stream, while hydrogen mass fraction is unity for the secondary stream. The exit boundary condition is obtained by second order extrapolation and is considered satisfactory for this problem dominated by supersonic flow. A purging time of 515 μs is used in the simulation as explained in Ref [6].

3. Numerical simulation

In the present study, OpenFOAM open source software [15] is used to carry out model free simulation. Unlike Direct Numerical

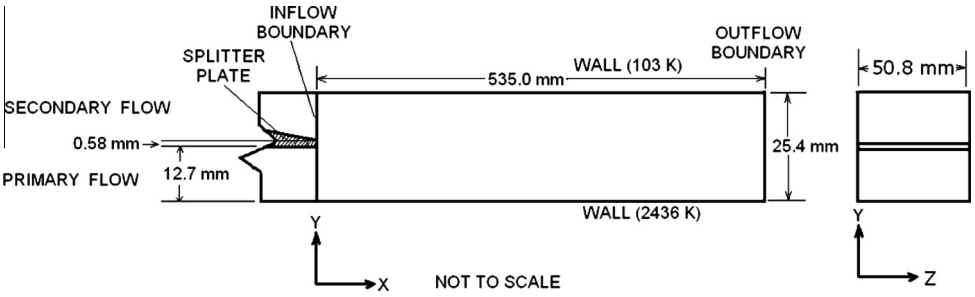

Fig. 1. Schematic of the Erdos [13] experimental mixing duct with details of duct cross section.

Table 1
Inflow parameters for non-reacting shear layer.

Location	Species	Velocity (m/s)	Temperature (K)	Pressure (Pa)	Mach number	Re (mm)
Primary	Nitrogen	3807	2436	27,580	3.99	2200
Secondary	Hydrogen	2389	103	27,580	3.09	42,000

Simulation (DNS), in a model-free simulation, the resolution of Kolmogorov scales is not sought for. However, the grid size in case of model-free simulation is such as to resolve the large-scale fluctuations affecting the formation and growth of mixing layer. Very small-scale fluctuations responsible for the transfer of turbulent mechanical energy to the thermal energy due to viscous effects may not be fully resolved. An extensive review of the model free simulation method and results for both non-reacting and reacting flows is provided by Givi [16]. This methodology of model free simulations has been used by many researchers and reported in literature. High resolution non-linear inviscid simulations were performed by Oh and Loth [14] for M_c values of 0.35, 0.45, and 0.7. The growth rate reduction with increasing M_c is well captured, the profiles of velocity, and turbulence intensities match satisfactorily with the experimental observations of Goebel and Dutton [17]. Oh and Loth [14] carried out the study of the mixing layers in a 2D domain, 400 mm long and 47.6 mm wide to match experimental test set up size of Goebel and Dutton [17]. Euler equations were solved using the argument that viscous effect does not play a dominant role in the mixing layer region. The finest grid consisted of 20,000 points with a minimum grid spacing of 0.3 mm. In another study involving the use of model free simulations, Risha [18,19] considered a 3-d domain of size 100 mm × 10 mm × 17 mm, and used a grid size of 100 × 53 × 35 for studying free mixing layers formed between two air streams at different convective Mach numbers (M_c = 0.2–1.56) and obliquity angles. The model free simulations carried out by Chakraborty et al. [9] shows a good match of the wall pressures for the mixing study of the confined compressible mixing layer. The grid independence of the solution was demonstrated by not only comparing the mean values of the various thermochemical profiles with different grids but also higher order quantities. A 1000 × 101 grid was shown to capture the features of the flow adequately. A good prediction of the different flow quantities in the compressible regime, by model free simulation technique makes it a suitable choice for the present study.

Instead of writing new software, open source libraries from OpenFOAM are customised to carry out 3D model free simulations. OpenFOAM is free-to-use open source numerical simulation software with extensive CFD and multi-physics capabilities. The governing equations are discretised using polyhedral Finite Volume Method. The object-orientation of the software facilitates easy model implementation in physical modelling and numerics (discretization, solvers, equation coupling). To the best of the knowledge of the authors, this may be the first attempt to apply OpenFOAM toolkit to solve high speed confined mixing layer.

The mass, momentum, energy and species equations are written in conservation form as

$$\frac{\partial \rho}{\partial t} + \nabla \cdot (\rho \vec{U}) = 0 \tag{1}$$

$$\frac{\partial \rho \vec{U}}{\partial t} + \nabla \cdot (\rho \vec{U}\vec{U}) = \nabla \cdot \sigma \tag{2}$$

$$\sigma = -\left(p + \frac{2}{3}\mu \nabla \cdot \vec{U}\right) I + \mu(\nabla \vec{U} + (\nabla \vec{U})^T) \tag{3}$$

$$\frac{\partial \rho h}{\partial t} + \nabla \cdot (\rho h \vec{U}) = \nabla^2(\alpha h) + \frac{Dp}{Dt} \tag{4}$$

$$\frac{\partial \rho Y_m}{\partial t} + \nabla \cdot (\rho Y_m \vec{U}) = \nabla^2(\mu Y_m) \tag{5}$$

The different transport coefficients and thermochemical properties are originally evaluated using Joint Army Navy Nasa Air Force (JANNAF) tables. However, the JANNAF tables contain the values only up to 5000 K temperature. In the present simulations, the temperatures are expected to rise above this limit. In this scenario NASA CEA400 tables have been included and used. These tables give the values of transport coefficients and thermochemical properties up to a temperature of 15,000 K.

The specific heat at constant pressure, enthalpy and entropy at a given temperature are evaluated using following relations [20]

$$\frac{C_p^0}{R} = a_1 T^{-2} + a_2 T^{-1} + a_3 + a_4 T + a_5 T^2 + a_6 T^3 + a_7 T^4 \tag{6}$$

$$\frac{H^0}{R} = -a_1 T^{-2} + a_2 T^{-1} \ \ln\ T + a_3 + a_4 \frac{T}{2} + a_5 \frac{T^2}{3} + a_6 \frac{T^3}{4} + a_7 \frac{T^4}{5} + \frac{a_8}{T} \tag{7}$$

$$\frac{S^0}{R} = -a_1 \frac{T^{-2}}{2} - a_2 T^{-1} + a_3 \ \ln\ T + a_4 T + a_5 \frac{T^2}{2} + a_6 \frac{T^3}{3} + a_7 \frac{T^4}{4} + a_9 \tag{8}$$

The constants a_1 to a_9 are listed by Gordon and McBride [21] at different temperature intervals and are provided as a data file named *thermo.inp* which is linked in OpenFOAM program for the evaluation of these thermodynamic quantities.

Similarily transport coefficients, namely thermal conductivity and viscosity are also evaluated through the suitable parametric

equations [21]. Schmidt number is assumed to be unity, which results in equal kinematic viscosity and species diffusivity.

The governing equations are discretised to obtain a linear system of equations, which can be solved by the CFD solver. OpenFOAM has its own programming language for writing solution algorithms for complex physics. It includes set of functions that describe standard differential operators $(\nabla^2, \nabla\cdot, \nabla, \nabla\times, \partial/\partial t, \partial^2/\partial t^2)$ which perform the discretization to create matrix equations. OpenFOAM offers different choice of methods for temporal discretization. For the discretization of the convective term, OpenFOAM offers many options. At run-time, the user can select the linear solver to be used to solve each matrix equation generated by a given application. The solvers are generalized so that the user can select the preconditioner and/or smoother for each solver.

For the model free simulations in the present work temporal discretization is done using second order backward scheme. Fourth order schemes are used for spatial discretization. Preconditioned Bi-Conjugate Gradient solver (PBiCG) is used for the solution of velocity, enthalpy, and species matrices with Diagonal Incomplete Lower Upper (DILU) preconditioner while Preconditioned Conjugate Gradient (PCG) solver is used for pressure and density matrices with Diagonal Incomplete Cholesky (DIC) preconditioner. Pressure Implicit with Splitting of Operators (PISO) algorithm is used for the coupling between pressure and velocity terms with two corrector steps. A maximum Courant number of 0.3 is observed to give stable simulations.

4. Results and discussion

The instantaneous and averaged values of axial velocity at different axial locations for without and with the presence of side wall are shown in Figs. 2 and 3 respectively. For the sake of clarity in the figures the scale has been started from 2400 m/s as the velocity of low speed stream, all the velocities lower than this value will be in black colour. In these figures the y- and z-axes represent lateral and span wise directions respectively. In the case where no side walls are considered, the three dimensionality of the instantaneous flow field is clearly observed in the axial velocity distributions, as shown in Fig. 2. Clemens and Mungal [22], and Sandham and Reynolds [23] have reported similar three dimensionality for convective Mach number (M_c) greater than 0.6 from experimental, DNS, and linear stability analysis. In the present study, the time averaged values can be observed to be two dimensional, as there are no geometrical or inlet flow conditions responsible for the introduction of three dimensionality in the flow field.

The three dimensionality of the instantaneous flow field can be clearly observed in the variation of the axial velocity along the span (z-direction), in case of the simulations carried out in presence of the side walls, as shown in Fig. 3. This three dimensionality in presence of side walls nullifies the argument that the flow field may have reduction in three dimensionality in presence of side walls. In fact, near the wall the flow field is more three dimensional in both instantaneous and averaged flow fields. This three dimensionality in the presence of side wall is further analysed for the normal component of Reynolds stress along the span and the pressure fluctuations at different points in span wise planes at 300 mm axial location.

The Reynolds stress in the span wise direction (σ_{zz}) is compared in Figs. 4 and 5, at axial locations of 300 mm and 400 mm respectively, for both with and without side wall configurations. The span-wise extent of the geometries is denoted by 'w', the values of σ_{zz} are taken at span-wise locations of $z = 0.2$w, 0.4w, 0.6w, and 0.8w. In the sidewall case, the wall is at the location $z =$ w. In an experimental study carried out by Gruber et al. [24] at an $M_c = 0.8$, the peak value of $(\sigma_{zz}/\rho\Delta U^2)$ is reported to be 3.7×10^{-4} compared to the value of 1.7×10^{-3} obtained in the present analysis. Although the M_c is same for both the studies, the experimental study of Gruber et al. [24] consider mixing of the same gas at static temperature difference of only 100 K with the mixing streams speeds of 500 and 91.2 m/s respectively. In the present case, the temperature difference is more than 2000 K, and the speeds of lower and upper streams are 3807 and 2389 m/s respectively. Higher velocities of streams in the present case will increase the Reynolds stress. Moreover, Gruber et al. [24] have taken free shear layer compared to the confined shear layer considered in the present study.

Examination of Figs. 4 and 5 indicates that the maximum difference in peak values of span wise normal Reynolds stresses are nearly 10% for both 300 and 400 mm axial locations for without side wall case, while this difference becomes around 25% for the cases where side wall is taken into consideration.

The examination of instantaneous fields of velocity and that of turbulence statistics, gives an impression that the side wall does not make the flow field to be two dimensional. On the other hand there is more three dimensionality introduced due to the presence of side wall. The normal Reynolds stress in the span wise direction clearly shows an increase in the values indicating three dimensionality of the flow field.

The behaviour of the flow field in the presence of side wall can be further examined by comparing the spectral content (amplitude and frequency of the flow quantities) of the two flow fields. The spectral content is examined at 9 different points in 300 mm and 500 mm axial locations as shown in Fig. 6. The coordinates of these points are shown in Table. 2 ('w' is the span wise width of the flow

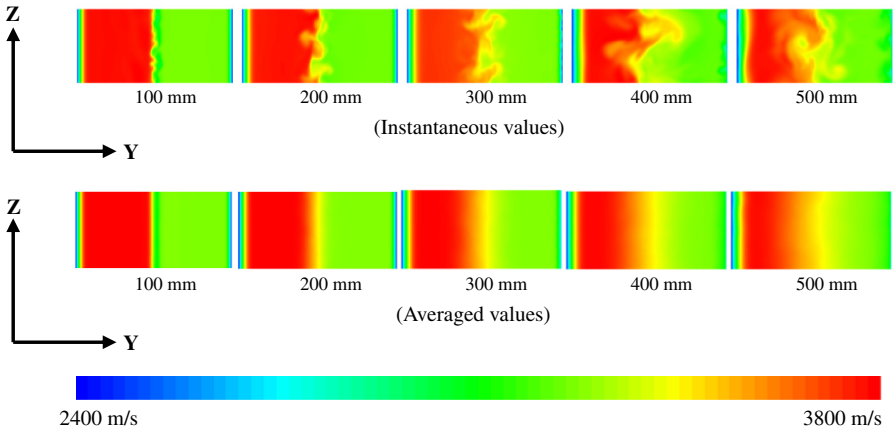

Fig. 2. Instantaneous and averaged distribution of axial velocity at different axial locations.

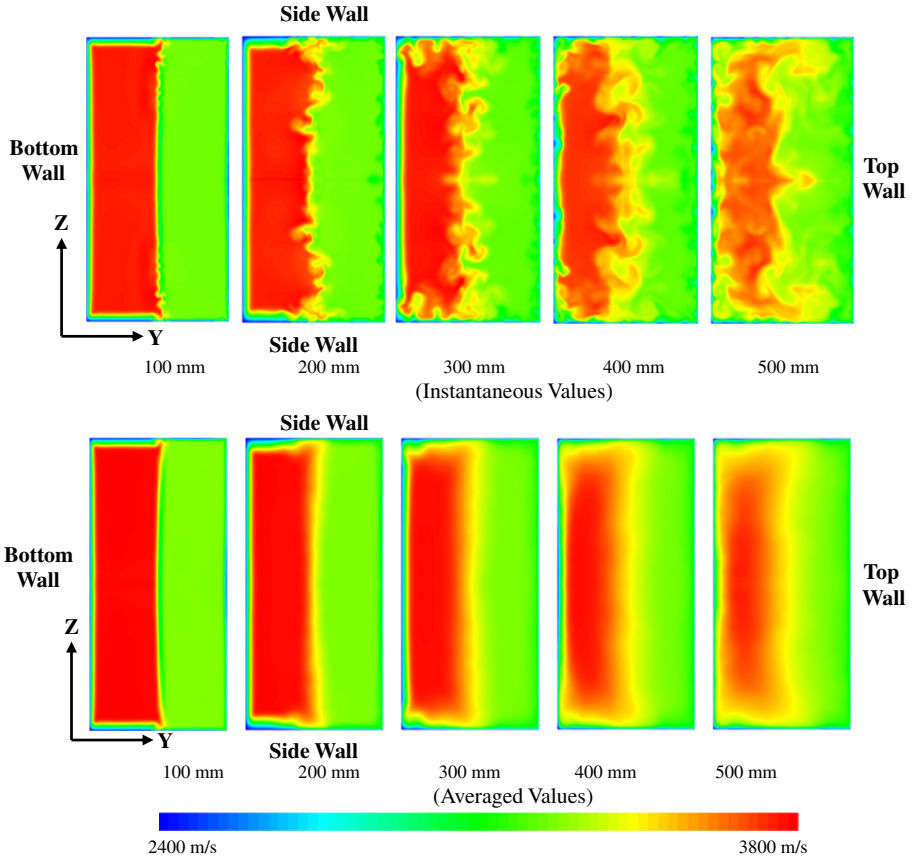

Fig. 3. Instantaneous and averaged distribution of axial velocity at different axial locations. The distance in z-direction is 50.8 mm and in y-direction is 25.4 mm. The results are reflected around the symmetry boundary (at $z = 0$) for the purpose of better visualisation.

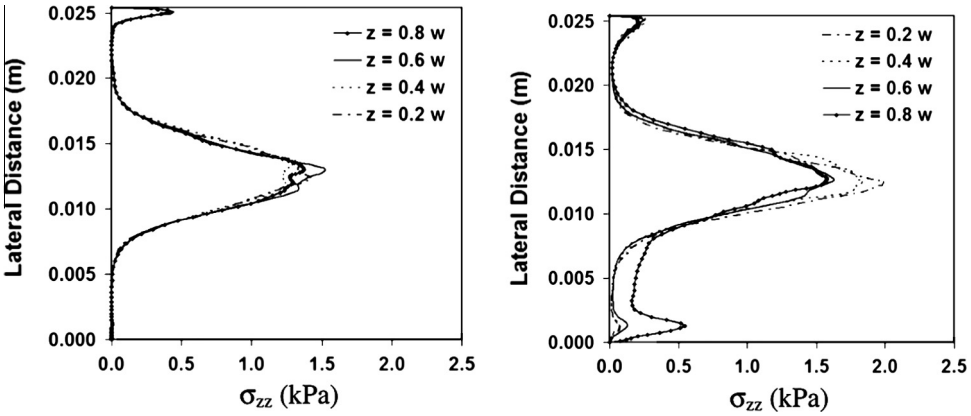

Fig. 4. Comparison of span wise component of Reynolds stress for simulations (a) without side wall and (b) with side walls at an axial location of 300 mm in the lateral direction.

duct). Points 1, 2 and 3 are in hydrogen side of the flow, and points 7, 8, and 9 are in the nitrogen side of the flow. Points 4, 5 and 6 are in the mixing layer region. Points 3, 6 and 9 are near the side wall in the side wall case simulations.

Pressure values are monitored at the selected points and the amplitude and frequency of the pressure values fluctuations are evaluated using FFT (Fast Fourier Transform). The amplitudes of the pressure fluctuations are normalized by the average values of pressures at the same points, and the frequencies are normalised by U_c/L, where U_c is the convective speed and L is the length of the duct. The convective speed defined as $(U_1a_2 + U_2a_1)/(a_1 + a_2)$, comes out to be 3006 m/s for this mixing layer. The pressure amplitudes with frequencies at different points are plotted in Fig. 7 for the cross sections at axial locations of 300. An examination of Fig. 7 shows that at points 1, 2 and 3 which lie within the hydrogen stream, the pressure fluctuations and the dominant frequencies are almost similar for both with and without side wall cases. Higher pressure fluctuations are observed for both cases in the mixing layer region as seen from the plots on points 4, 5, and 6 in Fig. 7. In the nitrogen side of flow as depicted in Fig. 7 by points 7, 8 and 9 again the frequencies and amplitudes are of the similar values for both the simulations.

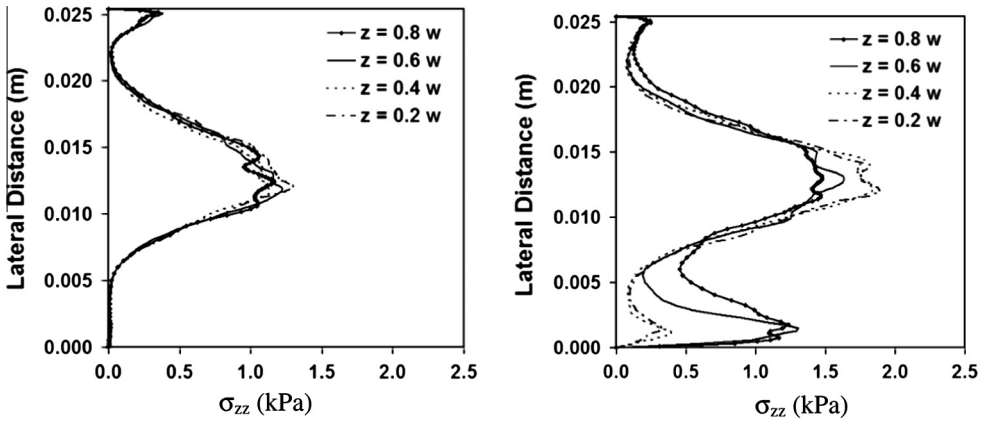

Fig. 5. Comparison of span wise component of Reynolds stress for simulations (a) without side wall and (b) with side walls at an axial location of 400 mm in the lateral direction.

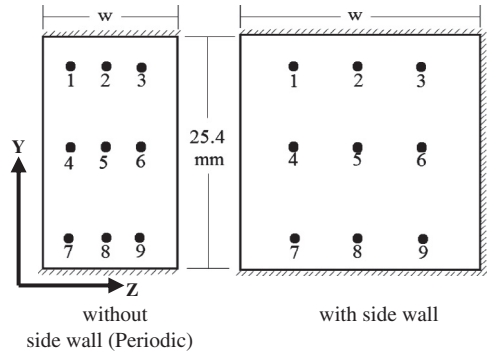

Fig. 6. Locations of points for the analysis of spectral content of without, and with side wall flow fields.

Further analysing Fig. 7, it can be observed that peak amplitude without side wall case for 300 mm axial location, remains constant at 1.5% of average pressure while the peak amplitudes varies between 1.4% and 2.3% in the mixing layer region (points 4, 5 and 6). These results demonstrate the effect of side wall in increasing the three dimensionality of the flow field.

Vorticity thickness defined as $\delta_\omega = \Delta U / \left(\frac{\partial u}{\partial y}\right)_{\max}$ is used to evaluate the shear layer thickness. The values of shear layer thickness for the present simulations along with the best fit in the linear region are shown in Fig. 8. The shear layer thicknesses from 2D simulations [6] are also plotted on the same figure for the sake of comparison. In the figure SPARK 2D indicate the 2D model free simulations carried out with a fourth order compact finite difference scheme [6]. It can be clearly seen that the linear region of the growth for OpenFOAM 3D simulation with side wall is nearly parallel to that predicted using the 2D simulations. The growth rate with side wall comes out to be 29.8 mm/m as compared with 30.2 mm/m predicted by SPARK 2D. The side wall seems to affect the growth rate to become nearly equal to that predicted using 2D simulations. The argument of side wall making the flow field two dimensional does not hold good in the light of flow data and turbulence statistics presented earlier. The reason for the growth rate reduction needs to be understood beyond the concept of two dimensionality in case of presence of side wall.

In a 2D mixing layer the disturbances are essentially two dimensional. It is possible that oblique disturbances, i.e. disturbances that propagate at an angle β to the mean-flow direction, exist in compressible shear layers. The angle β, usually called the oblique angle, is defined as the angle in the stream wise lateral plane relative to the positive stream wise direction. In the analytical studies of Lessen et al. [25] it is found that the shear layer becomes more unstable as β increases. Bogdanoff [26] proposes that in the turbulent shear layer the effect of β can be taken into account by defining an effective convective Mach number

$$M_{ceff} = M_c \cos \beta$$

The profound changes that a large value of β may bring can easily be appreciated: a flow with $M_c > 1$ may have $M_{ceff} < 1$. Since the disturbance is now characterized by M_{ceff} rather than by M_c, the entire flow is intrinsically subsonic, thus more unstable than one would predict using two-dimensional arguments.

In one of the studies of the effect of three dimensionality on the mixing layer growth rate Papamoschou [27] used concept of M_{ceff} along with the growth rate reduction correlation for compressible mixing layers to arrive at a relation between the growth rates of three dimensional mixing layers with that of corresponding 2D mixing layer. With the angle of oblique structure and convective Mach number the ratio of 3D growth rate with that of 2D growth rate is obtained using following relation.

$$\frac{\delta'_{3D}}{\delta'_{2D}} = \cos\ \beta \frac{f(M_c\ \cos\ \beta)}{f(M_c)} \tag{9}$$

where

$$f(M_c) = 0.18 + 0.82 \exp\left(-4M_c^2\right) \tag{10}$$

In the limit of $M_c \approx 0$ this relation (Eq. (9)) gives the ratio of 3D to 2D growth rates of incompressible mixing layer, which is always less than unity for nonzero values of β. The second term can be put as the ratio of compressible mixing layer growth rate at $M_c \times \cos\ \beta$ and M_c for 2D mixing layers. This growth rate ratio

Table 2
Location of points for the study of spectral content.

Point	1	2	3	4	5	6	7	8	9
Location (y,z) mm	20, 0.25w	20, 0.50w	20, 0.75 w	12.7, 0.25w	12.7, 0.50w	12.7, 0.75w	5, 0.25w	5, 0.50w	5, 0.75w

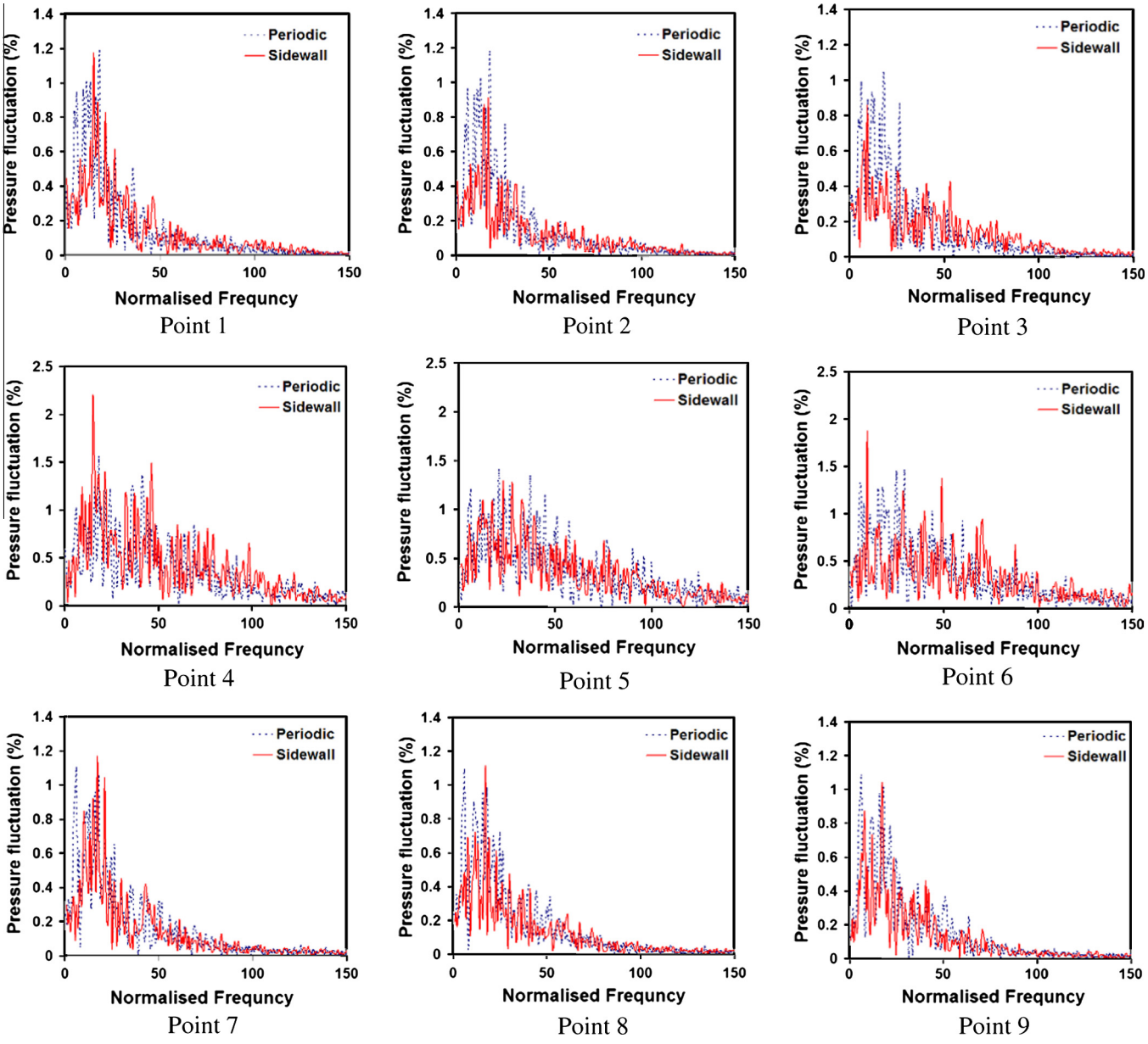

Fig. 7. Pressure fluctuations with frequencies at different points at an axial location of 300 mm.

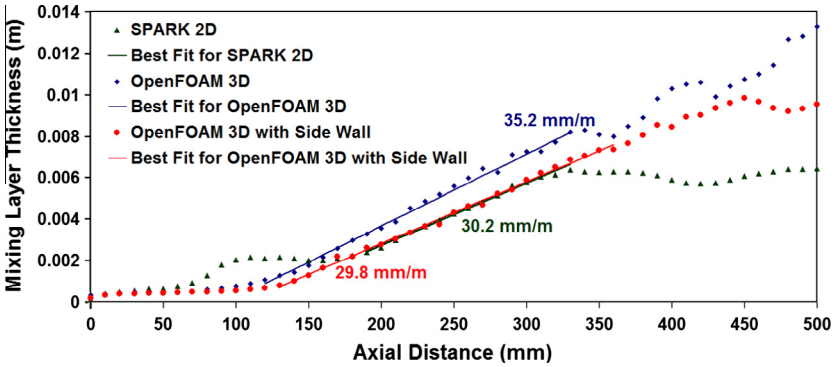

Fig. 8. Shear layer thicknesses and corresponding linear growth regions from different simulations.

depends strongly on the shape of function $f(M_c)$. For the shape of growth rate reduction curve considered by Papamoschou [27] The growth rate has been shown to reach around a maximum of 25% more in the region of $0.75 < M_c < 1.25$ depending on the obliquity angle of the structures in span wise direction. At all other M_c values the growth rate is shown to reduce due to presence of oblique

structures. It can also be shown that at low values of β (<20°) the difference between the 3D and 2D growth rates are minimal. This analysis gives a qualitative indication that the 3D growth rate when compared with 2D growth rate can show an increase or decrease depending on the obliquity angle β and the compressible growth rate ratio at $M_c \times \cos\beta$ and M_c.

In order to analyse the presence of oblique structures the top view at the middle plane in y-direction have been taken for hydrogen mass fraction for both without and with side wall simulations. These views are shown in Fig. 9a and b. In Fig. 9a the presence of 2D structures can be clearly noticed in the form of bands of colours in the initial upstream region. As the flow proceeds downstream the bands disintegrate in the span-wise direction also showing presence of there-dimensionality. However, these bands do not show any preferred directional orientation and hence there is no evidence of oblique structures. An examination of Fig. 9b shows a presence of oblique structures forming due to the presence of side wall. This oblique structure initially makes a small angle from the flow direction and attains a constant value of around 30° in the downstream direction. Similar observations can be made from the Fig. 9c and d on the distribution of magnitude of vorticity. The constant vorticity lines drawn in the side wall case also indicate a presence of oblique structures in the beginning of the flow as shown in Fig. 9e. The presence of this oblique structure may be responsible for the growth rate reduction in the side wall case.

The calculated reduction in the growth rate in presence of oblique structure due to Papamoschou [27], calculated based on 2D simulation $(\delta'_{3D}/\delta'_{2D}) = \cos 30^\circ \times (f(0.8\cos 30^\circ)/f(0.8))$ is 0.92, indicating a decrease due to the presence of the oblique structures. However, as discussed in Ref. [6], the growth rates of compressible shear layers predicted using 3D simulations, without the effect of side walls are higher than those predicted using 2D simulations. For the present geometry and flow conditions, the presence of side wall causes oblique structures to form and their effect is such as to cause a decrease in the growth rate of the compressible mixing layer. In totality the effect of side wall combined with three dimensionality results in only little variation from the 2D growth rate.

The presence of oblique structures due to wall can result either in increase or decrease in the growth rate when compared with two dimensional shear layer growth rate. It can be shown that except for a narrow band of M_c at certain values of β, the growth rate of 3D compressible shear layer is always less than that observed for corresponding 2D compressible shear layer. As seen in the Eq. (9), the first term $\cos\beta$ is always less than unity for nonzero values of β, the second term is always more than unity. Since the first term is dominating term resultant ratio remains less than unity for most of

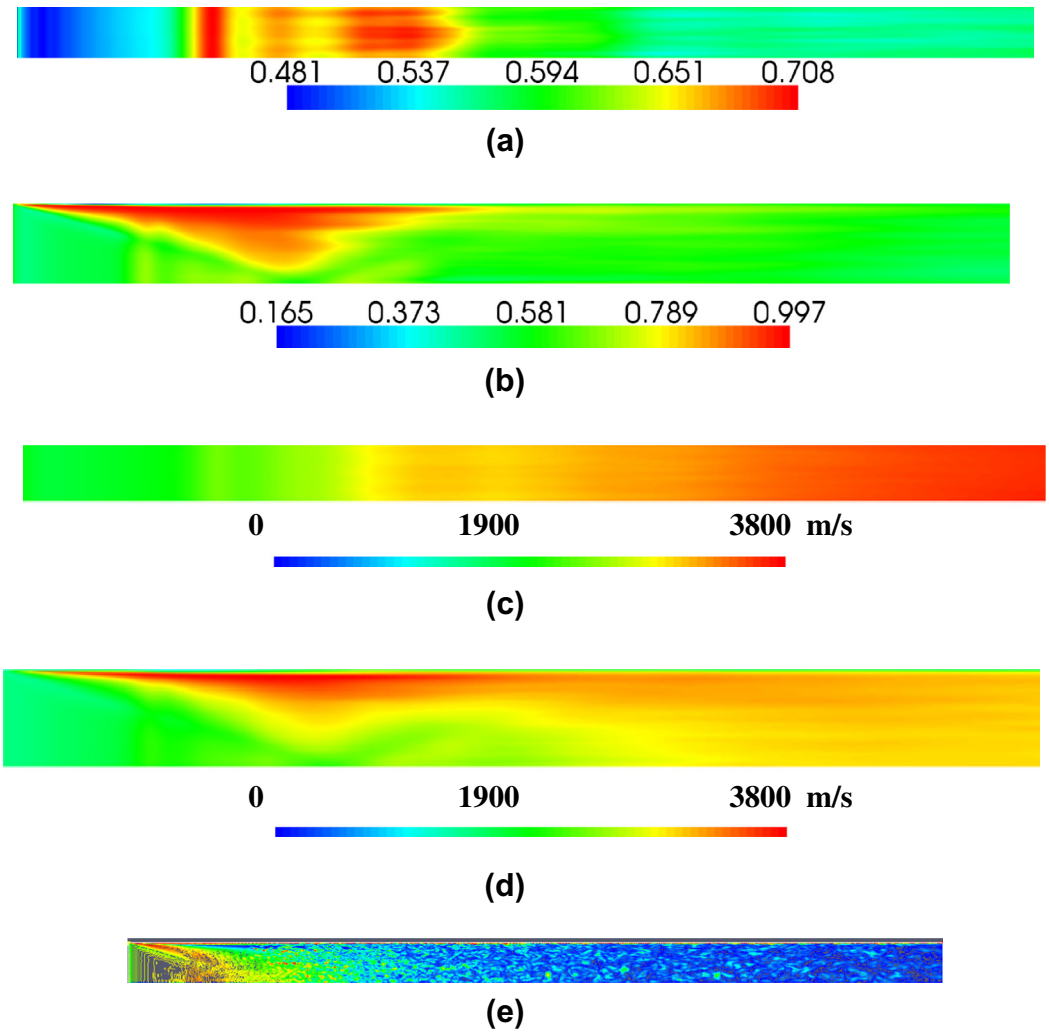

Fig. 9. Top view of the flow field showing hydrogen mass fraction distribution for (a) without side wall case (b) with side wall, magnitude of the velocity distribution for (c) without side wall case (d) with side wall, and (e) constant vorticity lines for side wall case. (Geometries are not to the scale).

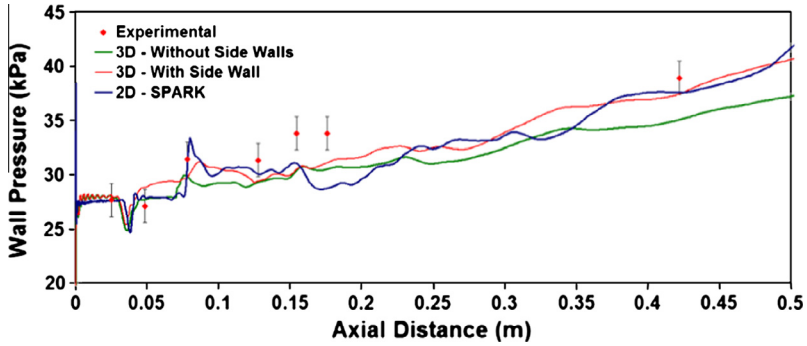

Fig. 10. Upper wall (hydrogen side) pressure comparison among experimental and numerical results.

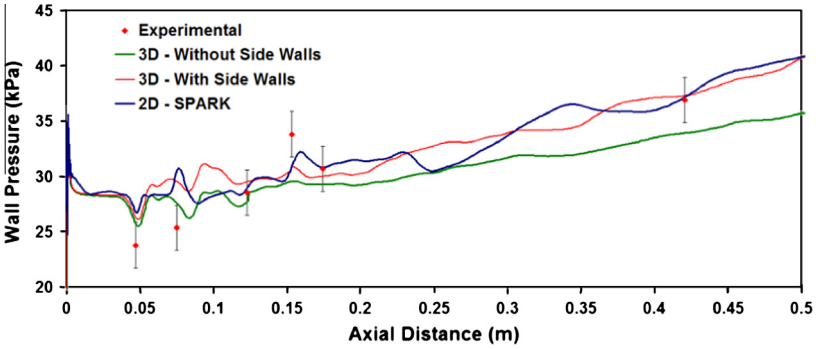

Fig. 11. Lower wall (nitrogen side) pressure comparison among experimental and numerical results.

the combinations of β and M_c. It is quite possible that for experimental studies, the shear layer growth rate reduces due to side wall oblique structure and the resultant shear layer growth rate is near to that evaluated using 2D simulations. Li and Fu [10], in their two dimensional simulations have observed that although the shear layer growth rate matches well with the experimental results, the experimentally observed fluctuations are not captured by the 2D simulations. From the present study, it appears that although the flow field and the statistics of the fluctuations remain three-dimensional, the combination of three dimensionality in the presence of oblique structure due to side walls, makes the 3D growth rate close to that obtained from 2D results.

The upper and lower wall pressures for with and without sidewall are shown in Figs. 10 and 11 respectively. The pressure values on the upper and lower walls for the sidewall case shows very good match with those obtained without any sidewall in the initial region of the flow. The pressure rise in case of sidewall simulation picks up in further downstream direction of the mixing duct. However the rise in pressure in the downstream direction is found comparably more than that obtained using the 3D simulations without any sidewall. The sidewall case pressure is found to be comparatively nearer to the 2D simulation pressures. The reason for this difference could be explained by the distribution of momentum in the third direction. In case of the presence of side wall this distribution of momentum in the third direction is restricted and reveals itself as increased pressure. Both in 2D case and the case with sidewall the momentum transfer in third direction is restricted. However, in case of the 3D mixing layer without side walls the momentum transfer in third direction keeps the resultant of all the velocity components higher and a lower wall pressure is observed.

5. Conclusions

Model free simulations with and without the presence of side walls for the Erdos' [13] experimental case have been carried out. Exact geometry of the flow duct used in the experimental study has been considered. A case with geometry without taking the side walls is also simulated. The turbulence statistics shows three dimensional nature of the flow for both the simulations. It has been shown that presence of side wall neither makes the flow field two dimensional, nor suppresses three dimensional disturbances. Instead an increased three dimensionality is observed as an effect of presence of side walls. However, the comparison of shear layer growth rate and wall pressures reveal a better match with the two dimensional simulation results. This better match is explained on the basis of formation of oblique structures due to the presence of side walls which also suppress the distribution of momentum in third direction making the pressures to be higher as compared with the case without side walls.

References

[1] Tam CKW, Hu FQ. Instabilities of supersonic mixing layers inside a rectangular channel. AIAA paper no. 88-3675-CP; 1988.
[2] Greenough J, Riley J, Soetrisno M, Eberhardt D. The effect of walls on a compressible mixing layer. AIAA paper no. 89-0372; 1989.
[3] Zhuang M, Dimotakis PE, Kubota T. The effect of walls on a spatially growing supersonic shear layer. Phys Fluids A2 1990;4:599–604.
[4] Morris PJ, Giridharan MG, Viswanathan K. Turbulent mixing in plane and axisymmetric shear layers. AIAA paper no. 90-0708; 1990.
[5] Chakraborty D. Confined reacting supersonic mixing layer – a DNS study with analysis of turbulence and combustion models. PhD thesis, IISc. Bangalore, India; 1998.
[6] Javed A, Chakraborty D, Paul PJ. Model-free simulations for compressible mixing layer. Proc Inst Mech Eng, Part G: J Aeros Eng 2013;227(6):977–91.
[7] Lu PJ, Wu KC. Numerical investigation on the structure of a confined supersonic mixing layer. Phys Fluids 1991;A3:3063–9.
[8] Liou T, Lien W, Hwang P. Compressibilty effects and mixing enhancement in turbulent free shear flows. AIAA J 1995;33(12):2332–8.
[9] Chakraborty D, Mukunda HS, Paul PJ. Two dimensional direct numerical simulation of nonreacting confined supersonic mixing layer. Aeronaut J 2000;June:291–6.
[10] Li Q, Fu S. Numerical simulation of high-speed planar mixing layer. Comput Fluids 2003;32:1357–77.
[11] Xu K, Prendergast KH. Numerical Navier–Stokes solutions from gas-kinetic theory. J Comput Phys 1994;114:9–17.

[12] Xu K. A gas-kinetic BGK scheme for the Navier–Stokes equations, and its connection with artificial dissipation and Godunov method. J Comput Phys 2001;171:289–335.
[13] Erdos J, Tamagno J, Bakos R, Trucco R. Experiments on shear layer mixing at hypervelocity conditions. AIAA paper 92-0628; 1992.
[14] Oh CK, Loth E. A numerical investigation of supersonic turbulent shear layers: compressibility effects. AIAA paper no. 94-2244; 1994.
[15] www.openfoam.com.
[16] Givi P. Model free simulations of turbulent reactive flows. Prog Energy Combust Sci 1989;15:l107.
[17] Goebel SG, Dutton JC. Velocity measurements of compressible turbulent mixing layers. AIAA J 1991;29(4):538–46.
[18] Risha DJ. Analysis of growth rates in three-dimensional air-to-air, supersonic shear layers using direct numerical simulation. AIAA paper no. 95-0523; 1995.
[19] Risha DJ. Analysis of turbulence statistics in three-dimensional, air-to-air supersonic shear layers using direct numerical simulation. AIAA paper no. 956072; 1995.
[20] Gordon S, McBride BJ. Computer program for calculation of complex chemical equilibrium compositions and applications – I. Analysis, NASA RP-1311; 1996. p. 20.
[21] Gordon S, McBride BJ. Computer program for calculation of complex chemical equilibrium compositions and applications – II. Users manual and program description. NASA RP-1311; 1996. p. 73.
[22] Clemens NT, Mungal MG. Two- and three-dimensional effects in the supersonic mixing layer. AIAA paper no. 1990–1978; 1990.
[23] Sandham ND, Reynolds WC. Compressible mixing layer: linear theory and direct numerical simulation. AIAA J 1990;28(4):618–24.
[24] Gruber MR, Messersmith NL, Dutton JC. Three-dimensional velocity measurement in a turbulent compressible mixing layer. AIAA paper 92-3544; 1992.
[25] Lessen M, Fox JA, Zien HM. On the inviscid stability of the laminar mixing of two parallel streams of a compressible fluid. J Fluid Mech 1965;23:355–67.
[26] Bogdanoff DW. Compressibility effects in turbulent shear layers. AIAA J 1983;21(6):926–7.
[27] Papamoschou D. Effect of three-dimensionality on compressible mixing. J Propuls 1992;8(1):247–9.